PNAS RESEARCH ARTICLE | CELL BIOLOGY

Regulated development of cannibalistic supergiant cells in the ciliate *Euplotes gigatrox*

Ben T. Larson[a,1], Daniele Giannotti[b], Mahara Mtawali[b], Samuel J. Lord[c], Vittorio Boscaro[b], and Patrick J. Keeling[b,1]

Affiliations are included on p. 11.

Edited by Julius Lukes, Akademie ved Ceske republiky, Ceske Budejovice, Czech Republic; received March 2, 2026; accepted April 3, 2026

Virtually all paradigms in developmental biology apply to differentiating cells and tissues within multicellular animals and plants. However, unicellular eukaryotes, which must simultaneously perform all activities necessary for a cell as well as an organism, also form complex and specialized structures, using exclusively subcellular processes. Here, we describe a ciliate (*Euplotes gigatrox* sp. nov.) undergoing drastic morphological transformations within a genetically uniform population, the most spectacular being the appearance of "supergiants" that increase in size, change shape, and modify their locomotion and feeding behavior to cannibalize clonal relatives. We explore supergiant formation from the perspective of life cycle, ecological strategy, and gene expression, demonstrating that supergiants are a distinct, regulated, transcriptionally unique stage. Differentiation appears to depend on internal and external conditions, suggesting that regulatory loops have evolved to ensure coupling between environmental and physiological conditions. This system provides a blueprint for approaching both cell differentiation and functional ecology in unicellular organisms, which might open new avenues for the generalization and contextualization of known morphogenetic mechanisms, as well as the discovery of new ones.

protist | morphogenesis | behavior | phenotypic plasticity | bet hedging

Significance

Development in microbial eukaryotes (protists), which can rival the morphological complexity of small animals, is largely unexplored. We report here on the finding that in clonal populations of the ciliate *Euplotes gigatrox* a small number of cells can develop into cannibalistic "supergiants" that drastically change size, shape, and behavior, transitioning from filter feeders to raptorial predators that can consume their kin. This process involves phenotypic tradeoffs and a system of regulatory loops consistent with a bet-hedging mechanism tuned to fluctuating environmental conditions. Our work introduces insights and approaches for studying morphogenesis and behavior in complex, unicellular organisms, complementing traditional studies of animal evolutionary developmental biology and cell differentiation.

Biological form is integrally tied to function, and all organisms across the tree of life acquire their morphological features through developmental processes. Our understanding of cell development and morphogenesis focuses primarily on the differentiation of cell types within multicellular organisms, and as a result the dominant models for the determination of cell shape and function mostly apply to animal and plant tissues. But the vast majority of eukaryotic diversity resides in unicellular protists (1), where the cell is the whole organism, facing many functional challenges within the confines of a single plasma membrane: moving, hunting, ingesting prey, escaping predators, finding a mate, but also replicating DNA, remodeling the cytoskeleton, harvesting energy, and managing vesicle trafficking, among other physiological processes (2, 3). The tissues of "complex" multicellular organisms compartmentalize functions and arise from the integration of highly specialized cell types, whose activities are generally each restricted to one primary role (4). This has become the paradigm for developmental biology, but it is in fact an exception both among extant organisms and throughout the history of life: protists must solve most of the same problems with organelles, membranes, and vesicles, rather than organs, tissues, and limbs (5). In contrast to prokaryotes, which excel at finding metabolic solutions, unicellular eukaryotes rely more on morphological and behavioral features, the complexity of which rivals those of small invertebrates (2, 3). Heterotrophic protists in particular respond to challenges with similar strategies but completely different tools than the more familiar animal models, allowing for comparisons between systems replete with both similarities and differences. Compared to developmental processes in animals, we know little of how unicellular body plans and morphological features form.

Among heterotrophic protists, ciliates are especially useful models because of their size, morphological complexity, and relative ease of cultivation, not to mention the uniqueness, among unicellular organisms, of their germline/soma separation (6); some have in fact provided insights in fields as disparate as cellular aging, regeneration, biophysics, and epigenetics (7–11). Ciliates of the genus *Euplotes* have attracted attention since the earliest days of microscopy, due to their ubiquity and striking features. *Euplotes* species occur in most aquatic ecosystems, and their movement, mating habits, symbiotic relationships, biogeography, and adaptations to local environments have all been extensively investigated (12–15). *Euplotes* cells have a highly ordered, complex animal-like body plan, with cilia packed into larger structures, called membranelles and cirri, that have been modified for feeding (by generating water currents), swimming, or to be used as "legs" for walking

Author contributions: B.T.L., D.G., M.M., S.J.L., and V.B. performed research; B.T.L., S.J.L., and P.J.K. contributed new reagents/analytic tools; B.T.L., D.G., M.M., S.J.L., and V.B. analyzed data; B.T.L. and P.J.K. conceptualized the project and provided supervision and project administration and acquired funding; V.B. conceptualized the project and provided supervision and project administration; and B.T.L., D.G., V.B., and P.J.K. wrote the paper.

The authors declare no competing interest.

This article is a PNAS Direct Submission.

[1]To whom correspondence may be addressed. Email: larsob3@rpi.edu or pkeeling@mail.ubc.ca.

This article contains supporting information online at https://www.pnas.org/lookup/suppl/doi:10.1073/pnas.2606891123/-/DCSupplemental.

Published May 14, 2026.

across substrates (Fig. 1*A*). The morphogenesis of these structures must be faithfully executed at each cell division, all while the cell largely remains active (moving, eating, etc.). This was once the subject of fascinating research that has largely been abandoned in the last 40 years, until a recent resurgence of interest (16–19).

One previously reported but seldom explored feature of certain ciliate species, including a few *Euplotes,* is the reversible transformation of cells within a genetically identical population into much larger "supergiants" that cannibalistically consume their relatives (20–24). The formation of supergiants raises several evolutionary, ecological, ethological, and physiological questions. Here we combine classical observations of morphological, ultrastructural, and behavioral changes with molecular and single-cell transcriptomic methods to show that *Euplotes* supergiants constitute a well-regulated developmental stage: they are differentiated cell types with specific morphology, behavior, and gene expression profiles,

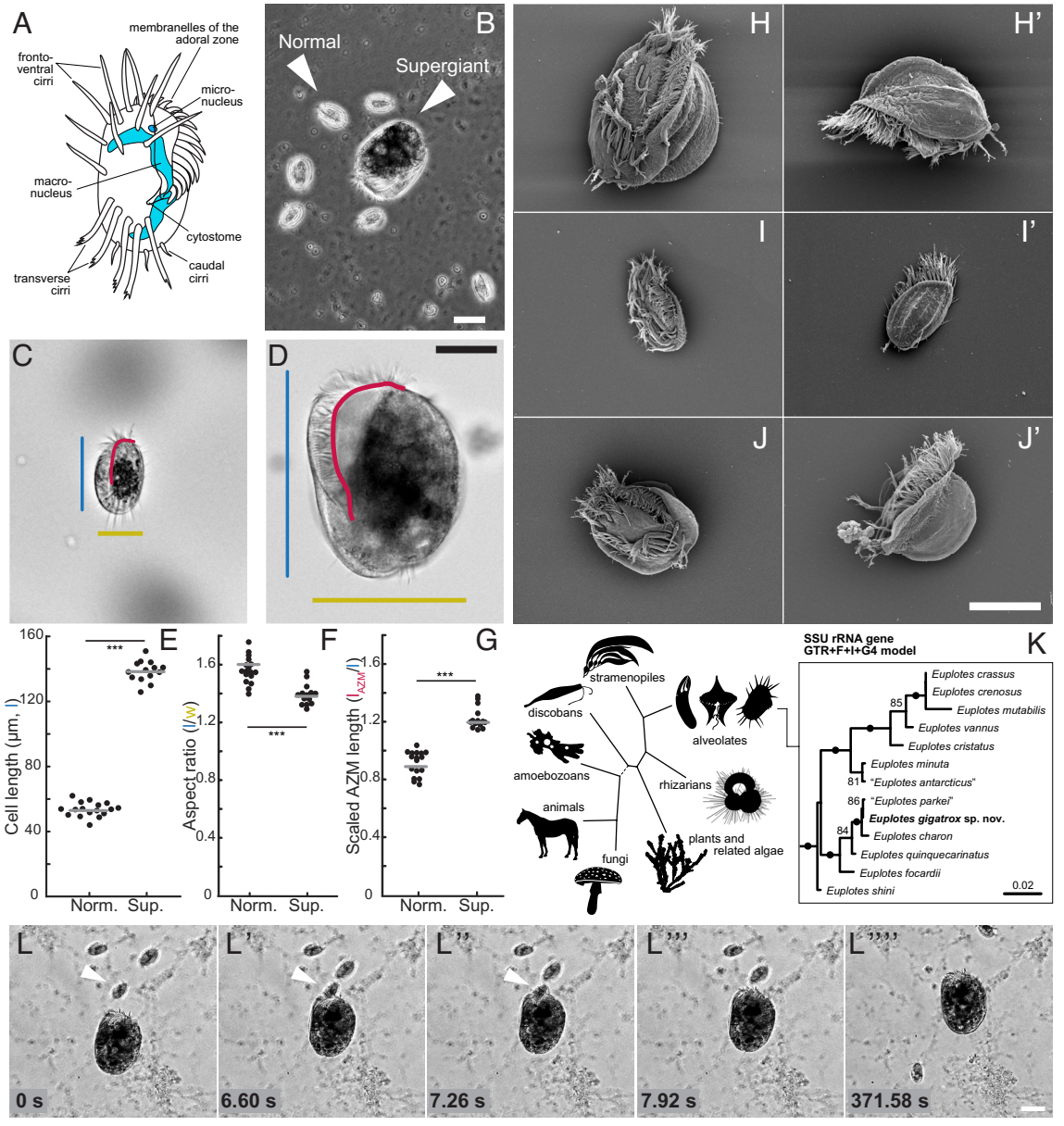

Fig. 1. *E. gigatrox* displays marked phenotypic polymorphism including supergiant cannibal cells. (*A*) A cartoon diagram illustrating basic cellular morphological characteristics of *Euplotes* species, including ventral cirri used for walking locomotion, membranelles (membranelles of the adoral zone, AZM) used to generate flows for swimming and feeding, sensory caudal cirri, and macro- and micronuclei. (*B*) A phase contrast image displaying genetically identical "normal" and "supergiant" morphs of *E. gigatrox* in close association in a culture flask. (Scale bar, 50 μm.) (*C*) Illustration of the morphological characterization of a normal morph with length in blue, width in yellow, and AZM length in red. (*D*) Illustration of the morphological characterization of a supergiant morph with length in blue, width in yellow, and AZM length in red. (Scale bar for both *C* and *D* = 50 μm.) (*E*) Comparison of cell lengths between normal morphs and supergiants demonstrates that supergiants are significantly larger (138.2 ± 4.3 μm vs. 53.6 ± 4.3 μm, mean ± SD). (*F*) Comparison of cell aspect ratios (cell length divided by width) between normal morphs and supergiants demonstrates that supergiants have a significantly less elongated cell body (1.4 ± 0.1 vs. 1.6 ± 0.1, mean ± SD). (*G*) Comparison of scaled AZM length (AZM length divided by cell length) between normal morphs and supergiants demonstrates that supergiants have an extended AZM relative to cell size (1.22 ± 0.08 vs. 0.91 ± 0.09, mean ± SD). In (*E*–*G*), measurements are from 17 normal morphs and 14 supergiants, *** indicates $P < 0.001$ by the two-sample *t* test, and gray bars indicate means. (*H* and *H'*) Scanning electron micrographs displaying ultrastructural morphology of supergiants. (*I* and *I'*) Scanning electron micrographs of normal morphs. (*J* and *J'*) Scanning electron micrographs of winged morphs. (Scale bar for *H*–*J'* = 50 μm.) (*K*) Phylogenetic placement of *E. gigatrox* in the tree of *Euplotes* (extracted from *SI Appendix*, Fig. S2; numbers close to nodes represent bootstrap support if above 75%, with dots indicating full support), and of *Euplotes* in the tree of eukaryotes. (*L*–*L''''*) Timelapse images from a video capturing a supergiant predation event on a normal morph prey cell, indicated by the white arrowhead. (Scale bar, 50 μm.)

induced both by external stimuli, as previously speculated (22, 23, 25), but also by their internal state. These features make *Euplotes* supergiants unique models for the comparative study of developmental biology mechanisms in unicellular organisms (17).

Results and Discussion

***Euplotes gigatrox* sp. nov. Displays an Extremely Polymorphic Phenotype.** While surveying protist diversity on the Caribbean island of Curaçao, we collected *Euplotes* cells from a seawater filtration system that draws its supply from near-shore waters. The ciliates were initially coisolated with other microbial eukaryotes and bacteria. To establish laboratory cultures, we manually picked *Euplotes* cells and placed them in nutrient-supplemented artificial seawater along with co-occurring bacteria, which serve as a food source. Cultures were kept at 20 °C and passaged approximately once per month. After several months, especially large cells began to appear sporadically (supergiants, Fig. 1*B*). These supergiants are morphologically distinguishable from the abundant "normal" cells by their large size (cell length = 138.2 ± 6.4 μm vs. 53.6 ± 4.3 μm), less elongated cell bodies (cell aspect ratio = 1.4 ± 0.1 vs. 1.6 ± 0.1), and extended area of the oral (feeding) membranelles (scaled membranelle region length = 1.22 ± 0.08 vs. 0.91 ± 0.09, Fig. 1 *C–I*). Despite differential scaling of cell size and shape, we observed that supergiants retained the same number of ventral cirri (bundles of cilia) as normal morphs (Fig. 1 *H–I*). Upon closer inspection, we also noted further morphological diversity in the cultures, including "winged" morphs (Fig. 1*J*), which might serve a defensive purpose (26, 27), as well as cells that appeared intermediate between the normal and supergiant phenotype (*SI Appendix*, Fig. S1). It was impossible to unambiguously categorize intermediate cells into well-defined, cohesive groups based on gross morphology, and we hypothesized that they represent progressive stages in supergiant development.

Phylogenetic analysis of the small subunit (SSU) ribosomal RNA gene and morphological comparisons confirmed that this *Euplotes* isolate belonged to a previously undescribed species (Fig. 1*K*; see *SI Appendix*, Fig. S2 and *SI Text* for a more detailed species characterization), which we name *E. gigatrox,* in reference to the presence of fierce, supergiant cells.

Supergiants Exhibit Altered Behavioral Patterns. Larger cells in clonal cultures have been observed in many ciliates, and are often associated with cannibalistic feeding (22, 24, 25). The supergiants of *E. gigatrox* were also observed to consume clonal relatives (Fig. 1*L* and Movies S1 and S2) at a rate of up to approximately 1 prey every 10 min. In cannibalistic feeding, predator cells "run over" their smaller kin until they are lodged in the oral cavity, where they are engulfed. This contrasts sharply with filter feeding in normal morphs and other *Euplotes* species, where a current is generated by the oral membranelles to pull bacteria and small protists in. The behavioral and structural differences between normal cells and supergiant cannibals offer fascinating eco-evolutionary and developmental implications, so we sought to characterize them in more detail.

We found that supergiants exhibit distinct motility patterns. Freely behaving normal morphs under dilute environmental conditions display the expected range of cell movements (15, 28), including walking over the substrate at various speeds as well as swimming along helical trajectories in fluid (Fig. 2*A* and Movie S3). Supergiants, in contrast, only walk, often along curling trajectories, and spontaneous swimming was never observed (Fig. 2 *B* and *C* and Movie S4). Instantaneous velocities of walking supergiants show generally higher speeds, but also a much broader distribution compared to the speeds of normal morphs, despite the fact that the latter can both walk and rapidly swim (*Materials and Methods* and Fig. 2*C*). The turning angle distribution (*Materials and Methods*) of supergiants displays a shoulder at around 30 degrees due to the persistent curvature of many trajectories, while the turning angle distribution for normal morphs exhibits a single peak and no shoulder, consistent with prior analyses of other *Euplotes* species (15) (Fig. 2*D*). We also examined the mean square displacement (MSD) of cell movement patterns (*Materials and Methods*), which is commonly used to characterize trajectories (29). Normalized MSD curves for both morphs display similar initial scaling exponents of 1.43 (95% CI bounds: 1.41 to 1.46; R^2 = 0.9977) and 1.70 (95% CI bounds: 1.69 to 1.71; R^2 = 0.9998) respectively. This corresponds to directionally biased movement at short timescales, although the increasing slope transitioning to smaller scaling exponent of 0.30 (95% CI bounds: 0.28 to 0.32; R^2 = 0.6063) of supergiants illustrates the transition from directed movement at subsecond timescales to confined movement over seconds to tens of seconds timescales (all fits computed using the Curve Fitter application in Matlab). Taken together, the properties of supergiant trajectories, including higher speeds (Fig. 2*C*) and constrained directed motion (Fig. 2 *D* and *E*), are consistent with local search patterns, where cells efficiently scout their immediate surroundings, increasing their chance of prey encounter. Notably, in 2D environments, particularly those with complex topography or obstacles, subdiffusive search patterns tend to be optimal for target finding, whereas in open 3D environments, ballistic or superdiffusive search patterns tend to be more effective (30). Indeed, the putative search patterns observed here are reminiscent of those exhibited by some animals and protists and used in some robotics contexts for 2D search strategies (31–37). In other words, *E. gigatrox* shift behaviorally to movement patterns consistent with hunting surface-crawling conspecifics as they change their cell size and shape accordingly.

We hypothesized that the larger bulk, more irregularly shaped cell bodies, and denser composition all reduce the efficiency of swimming in supergiants. To test this, we gently disturbed cells that were walking on glass-bottomed Petri dishes by pipette aspiration or by shaking the dish. We then recorded the resultant trajectories of cells as they moved through the fluid (Movie S5). Supergiants do not appear to be able to swim very far, often tumbling while moving in an undirected fashion, in contrast to the directed, helical swimming of normal morphs documented in this and other *Euplotes* species (28, 38) (Fig. 2 *F* and *G* and Movie S5). Scaled swimming distances, calculated by taking the ratio of the integrated distance traveled by the cell to the total distance traveled from the start to the end of the swimming trajectory, are significantly smaller for supergiants compared to normal morphs (Fig. 2*H*). These results suggest supergiants have reduced swimming performance in terms of long-range dispersal ability. In principle, swimming allows cells to better explore 3D environments, whereas walking is restricted to surfaces. Supergiant formation therefore may represent a tradeoff where cells can feed on locally available prey items that would otherwise be inaccessible while sacrificing motility over extended distances, perhaps as a strategy to capitalize on ephemeral local conditions. This adaptation is a departure from the more commonly reported "swarmers" or dispersal forms of ciliates and other protists, where under stressful conditions cells become more efficient long-distance swimmers, supposedly for rapid dispersal to favorable environments (39–41).

Supergiants Result from Differentially Regulated and Reversible Developmental Pathways. We next sought to investigate conditions under which supergiants form. Many organisms, including protists, undergo life history transitions in response

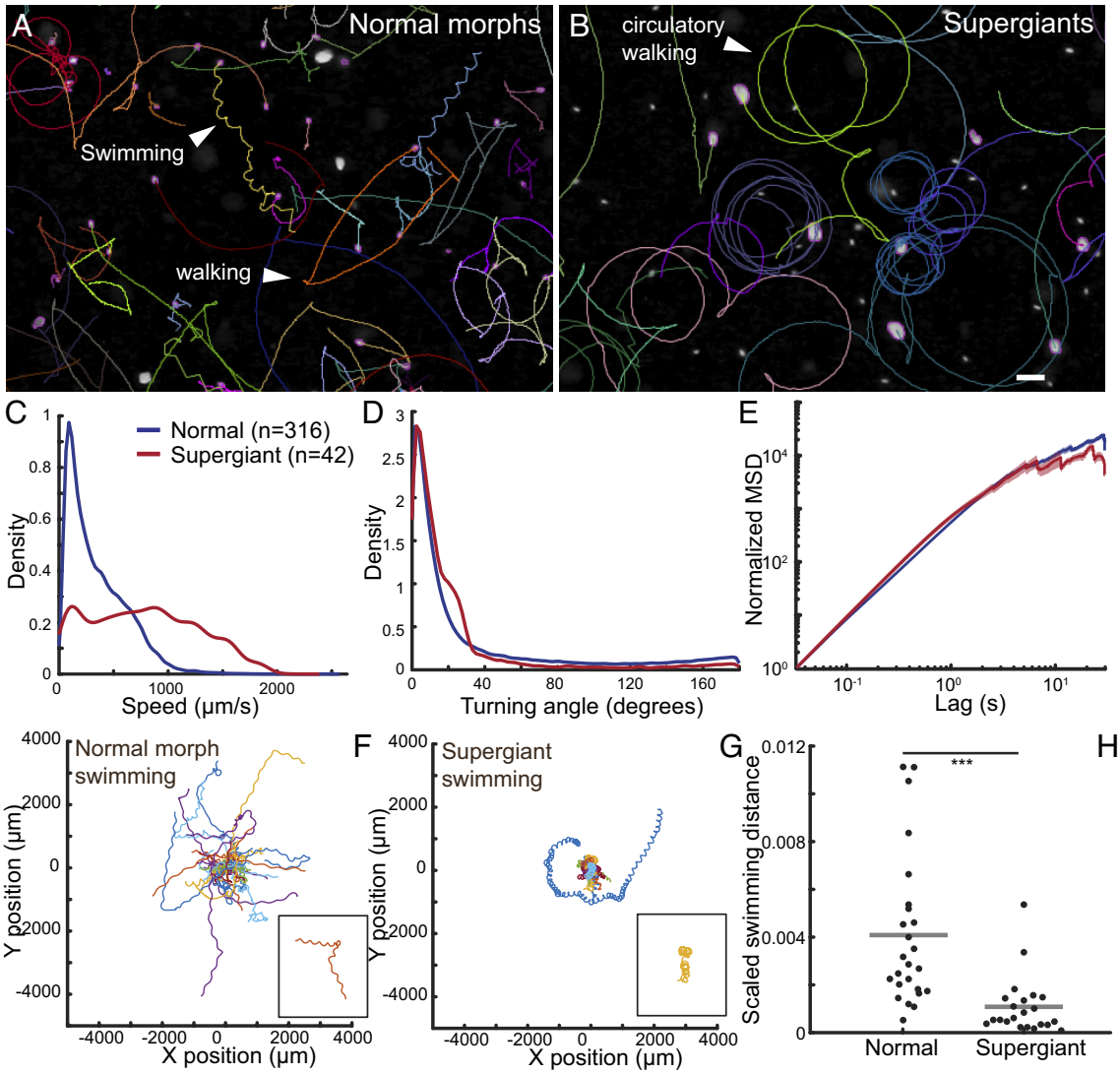

Fig. 2. Supergiant formation involves a tradeoff between raptorial feeding and swimming. (*A*) Representative trajectories of freely behaving normal morphs display helical swimming and linear walking paths. (*B*) Representative trajectories of freely behaving supergiants (from the same sample as *A*) illustrate curling or circulatory paths, which are less common in normal morphs. Different colors in panels *A* and *B* indicate trajectories of different cells and are randomly applied. (Scale bar for *A* and *B* = 200 μm.) (*C*) A probability-density plot of speeds of freely behaving normal morph and supergiant cells shows that supergiants tend to move at higher speeds. Speed (y-axis) refers to pooled frame to frame instantaneous speeds (*Materials and Methods*). (*D*) A probability-density plot of turning angles along cell trajectories of freely behaving normal morph and supergiant cells shows supergiant trajectories have different characteristic curvature corresponding to spiraling movements displayed in panel *B*. For each group of cells, the probability-density estimates in panels *C* and *D* were obtained using the ksdensity function in Matlab. (*E*) Normalized MSD of freely behaving normal morph and supergiant cells shows that each morphotype has similar dispersal characteristics over time, although more rapid decrease in slope of the supergiant MSD curve compared to normal morphs indicates confinement of trajectories over seconds to tens of seconds timescales. Solid lines represent mean MSDs and shaded regions (barely visible) indicate bootstrapped 95% CI. Measurements for (*C*–*E*) are pooled from n = 316 normal morph and n = 42 supergiant cells from three separate samples. (*F*) Trajectories of swimming normal morphs after they have been gently displaced from the coverslip on which they had been walking display expected extended helical trajectories with occasional turns. These trajectories are pooled from 25 different cells from three different samples and are mean centered. (*G*) Trajectories of swimming supergiants after they have been gently displaced from the coverslip they had been walking on show compact helical swimming and tumbling. These trajectories are pooled from 22 different cells from three different samples and are mean centered. Colors in *F* and *G* are applied randomly and designate different individual cells. (*H*) Scaled swimming distances calculated by taking the ratio of the distance from the start to the end of the trajectory divided by the total integrated distance traveled by normal morphs and supergiants displayed in panels *F* and *G*. Gray bar indicates the mean. *** indicates $P < 0.001$ by the two-sample *t* test.

to environmental cues. Indeed, phenotypic plasticity in response to predators, including identification of specific signals in the form of predator-secreted compounds, has been described in several species of *Euplotes* (42–44). Cannibal formation triggered by environmental conditions has also been reported in other ciliates, notably *Blepharisma* (20). Starvation is generally proposed as the inducing trigger, although systematic studies have rarely been undertaken. While we observed a consistent yet sporadic appearance of supergiants in our cultures, no obvious trend in culture conditions or timing was apparent. We therefore tested a range of environmental variables including prey abundance, prey type (including bacteria and eukaryotic algae), salinity, temperature, population density, and conditioned media (*SI Appendix*, Table S1). Contrary to previous reports (22), these tests were inconclusive, with supergiants continuing to form sporadically under various conditions with the exception of complete starvation. To test the dynamics of supergiant appearance under more controlled conditions, we grew cells in different concentrations of red algae culture medium (RA). This growth medium serves primarily as a carbon and nutrient source for bacterial prey cocultured with *Euplotes*. We found that supergiants consistently began to form as a population entered

stationary phase following exponential growth, then increased in abundance before ultimately disappearing (Fig. 3 *A* and *B*). During all these experiments, supergiants never amounted to more than 5% of the population, which suggests that supergiant formation is a low-probability life history transition. Supergiants did not form in the complete absence of nutrients and prey bacteria, probably because cell growth and division cannot be sustained (Fig. 3*B*). Surprisingly, they also did not form under high nutrient conditions (Fig. 3*B*). Prior to the appearance of supergiants, we often observed cells of intermediate size with extended oral apparatuses and rapid motility (*SI Appendix*, Fig. S3 and Movie S6). These cells can also feed cannibalistically (Movie S6) and may represent

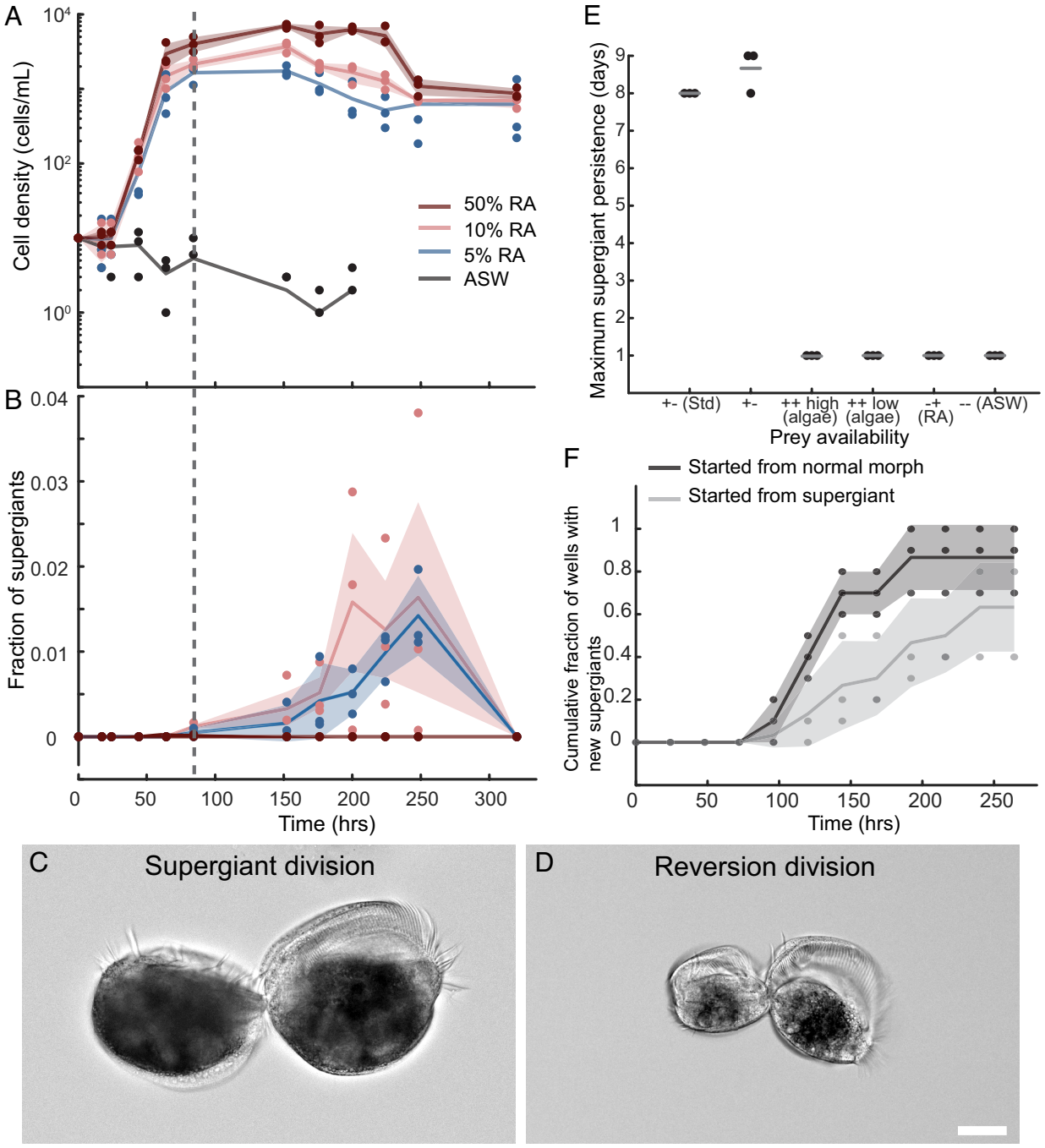

Fig. 3. Supergiants form and revert under specific environmental conditions in a history-dependent manner. (*A*) Growth curves of cells in different media enrichment conditions, denoted by different colored curves and points. (*B*) Fraction of supergiants over time corresponding to the same cell populations in panel *A*. In both *A* and *B*, points indicate independent experiments from three trials, solid lines are means, and shaded region indicates SEM. Note that supergiants only appeared in 5% and 10% red algae media (RA). The vertical dashed line indicates the first appearance of supergiants. (*C*) Supergiants can propagate supergiants by dividing approximately equally, as depicted in this representative example of cells just prior to separating during cytokinesis. (*D*) Supergiants revert to normal morphs by a series of asymmetric cell divisions. This image captures an intermediate stage of this reversion process just prior to cells separating during cytokinesis. (Scale bar for *C* and *D* = 25 μm.) (*E*) Supergiant persistence under varied environmental conditions. Results are reported for N = 3 for each condition. +− (Std) = induction in 15% RA; +− = supergiants and normal morphs in ASW, ++ high (algae) = cells fed with a 1:10 dilution of algal prey; ++ low (algae) = cells fed with a 1:100 dilution of algal prey; −+ (RA) = supergiants in 15% RA with no normal morphs; −− = supergiants in ASW. (*F*) Cumulative fraction of wells in a well plate that contain supergiants in populations started from either a single normal morph or a single supergiant in 10% RA media shows that populations started from supergiants form new supergiants more slowly and are less likely to produce supergiants overall. Each experiment involved ten wells seeded by an individual cell; points indicate results from an individual experiment, solid lines represent the mean, and shaded regions represent the SEM.

a step in the supergiant developmental pathway. In addition to arising from a developmental process from normal morphs (Movie S7), we also found that supergiants can propagate themselves through approximately equal cell divisions (Fig. 3*C*). We then documented the process of reversion to the normal cell type, which takes place through asymmetric cell divisions (Fig. 3*D*). While exploring conditions under which supergiants form, we noticed that supergiant persistence tended to differ across environmental conditions. Under conditions where normal morphs are present but few small prey items are available (including induction in RA and cells placed in artificial seawater), supergiants persisted for up to 8 d (Fig. 3*E*). In contrast, when small prey items that can be consumed by normal morphs are abundant, or when no normal morphs are available for cannibalistic consumption, supergiants persist for no more than a day (Fig. 3*E*).

A less explored possibility is that internal cellular states, in addition to external prompts, play an essential role in triggering or suppressing supergiant formation, as is the case for life history transitions in some other protists (41). Experiments reported in Fig. 3 *A* and *B* suggested that growth history in particular may play a role. Supergiants do not form when cells are subjected to starvation in media free of additional nutrient supplements (artificial seawater, ASW), and slowing cell proliferation alone is not sufficient to induce supergiant formation. Experiments summarized in *SI Appendix*, Table S1 further demonstrated that supergiant formation is not unique to growth conditions under low RA concentrations and therefore, is unlikely to be induced exclusively by specific environmental cues as is the case for life history transitions in other protists (45, 46). We hypothesized that environmental conditions as well as growth state might influence supergiant formation. To investigate whether the disposition to form supergiants is history-dependent, we picked individual cells of normal morphs and supergiants and placed them in wells containing either RA medium at a concentration compatible with supergiant formation, or ASW. In both ASW and RA conditions, all supergiants reverted to normal morphs within 24 h (n = 10, N = 3 for both conditions). In ASW, individual supergiants produced up to nine normal morphs in 24 h, and up to 16 normal morphs over 120 h, whereas individual normal morphs underwent a maximum of one binary cell division in 24 h and then stopped dividing. In RA, cells proliferated as expected based on standard culture conditions. Supergiants formed earlier and with higher overall frequency in populations started from normal morphs compared to those started from supergiants (Fig. 3*F*). That is, cells recently reverted from the supergiant state do not have the same potential to form supergiants compared to cells produced by normal morphs randomly sampled from a population. These results support the hypothesis that supergiant formation depends on the internal, growth history-dependent, cellular state, and suggest that supergiant reversion may trigger a latency or cool-down period, likely by temporarily suppressing the pathways that promote the transition.

Taken together, these results are consistent with supergiant formation being a low-probability life history transition that occurs after a period of recent cell proliferation when small prey items are not too abundant and large prey items are present and is less likely to occur in cells that have recently reverted from the supergiant state. Supergiant formation, reversion, and propagation therefore are cyclic regulated processes, controlled by environmental conditions as well as history-dependent, internal cell states.

Development of *E. gigatrox* Correlates with Gene Expression Profiles. To investigate the molecular basis of supergiant formation and reversion, we sequenced single cell transcriptomes from 41 *E. gigatrox* cells corresponding to supergiants (n = 9), normal morphs (n = 10), normal morphs that had recently reverted from the supergiant state (n = 10), and "intermediates" (n = 12) whose appearance did not match that of either normal or supergiant cells (*SI Appendix*, Fig. S1), and that we hypothesize represent a heterogeneous group of transitional states. After all sequences were clustered and contamination filtered out, 35,567 distinct transcripts were identified for a total length of 38.3 Mbp, corresponding to 27,557 protein-coding genes (Dataset S1).

An initial count matrix (Dataset S2) was used to examine the variance and distribution of genes represented in different libraries through principal component analysis (PCA; Fig. 4*A*). PCAtest (47) confirmed the overall statistical significance of the analysis as a whole and of the first six principal components (PCs) (Dataset S3). PC1 and PC2 combined covered 43.6% of the total variance. Normal and supergiant cells both form strongly supported clusters, and more surprisingly so do normal morphs that recently reverted (Fig. 4*A*), demonstrating a molecular basis for the latency period observed during growth experiments. The pattern is supported by a global ANOSIM test on the whole dataset ($R = 0.616$, $P = 0.001$), and even more strongly when "intermediate" cells, which are expected to be a less coherent category, were excluded ($R = 0.8537$, $P = 0.001$), as well as by pairwise ANOSIM tests (Dataset S3). These results suggest that the processes of cellular differentiation to form supergiants, and dedifferentiation to reverted and normal stages, are both underpinned at the molecular level by modulating gene expression profiles.

A gene-cluster analysis (Fig. 4*B*) of the 50 genes with the highest expression variance associated with the three distinct developmental conditions (normal, supergiant, and reverted) identified two sets of differentially expressed genes: one set is switched on during the differentiation to supergiants, and partially lingers in the reverted stage, while a second set is upregulated in reverted cells only, and it likely accounts for the latency period. The same pattern is retrieved, albeit less distinctly, when the 500 genes with the highest variance were analyzed (*SI Appendix*, Fig. S4).

The putative functions of these genes were assessed from 7,900 out of 27,557 predicted coding sequences annotated using the eggNOG v5 database and 18,871 coding sequences annotated with InterProScan (Dataset S4). To detect genes that are most relevant for the transitions, we first identified those that contribute more to the variance in the first two components of the PCA by measuring their loading score indices and correlation significance (Dataset S5). Twenty genes with the highest positive and 20 with the lowest negative loadings scores were selected for both PC1 and PC2, and, for each gene, their expression levels were compared across the different conditions (Dataset S6). Genes involved in chromatin structure and dynamics were the most represented category, including genes coding for histones H2A, H2B, H4, and a protective telomere end-binding protein, all of which were upregulated in supergiant and reverted cells compared to normal cells. The annotated gene with the absolute highest loading score codes for a cyclin-dependent kinase regulatory subunit, which also appeared downregulated in normal cells. These observations suggest strong regulatory ties between cell differentiation and genes commonly associated with the cell cycle.

The total number and extent of differentially expressed genes between each developmental condition pair was visualized through pairwise matrices, each including a different subselection of genes (Dataset S7). No less than 42% of all genes are differentially expressed in each comparison, and the differences are both wide and statistically significant (Fig. 4*C*), suggesting that many genes are involved in the transitions. Noticeably, in reverted cells relative to normal cells, most genes were upregulated, reflecting the same pattern as the cluster analysis (Fig. 4*B*).

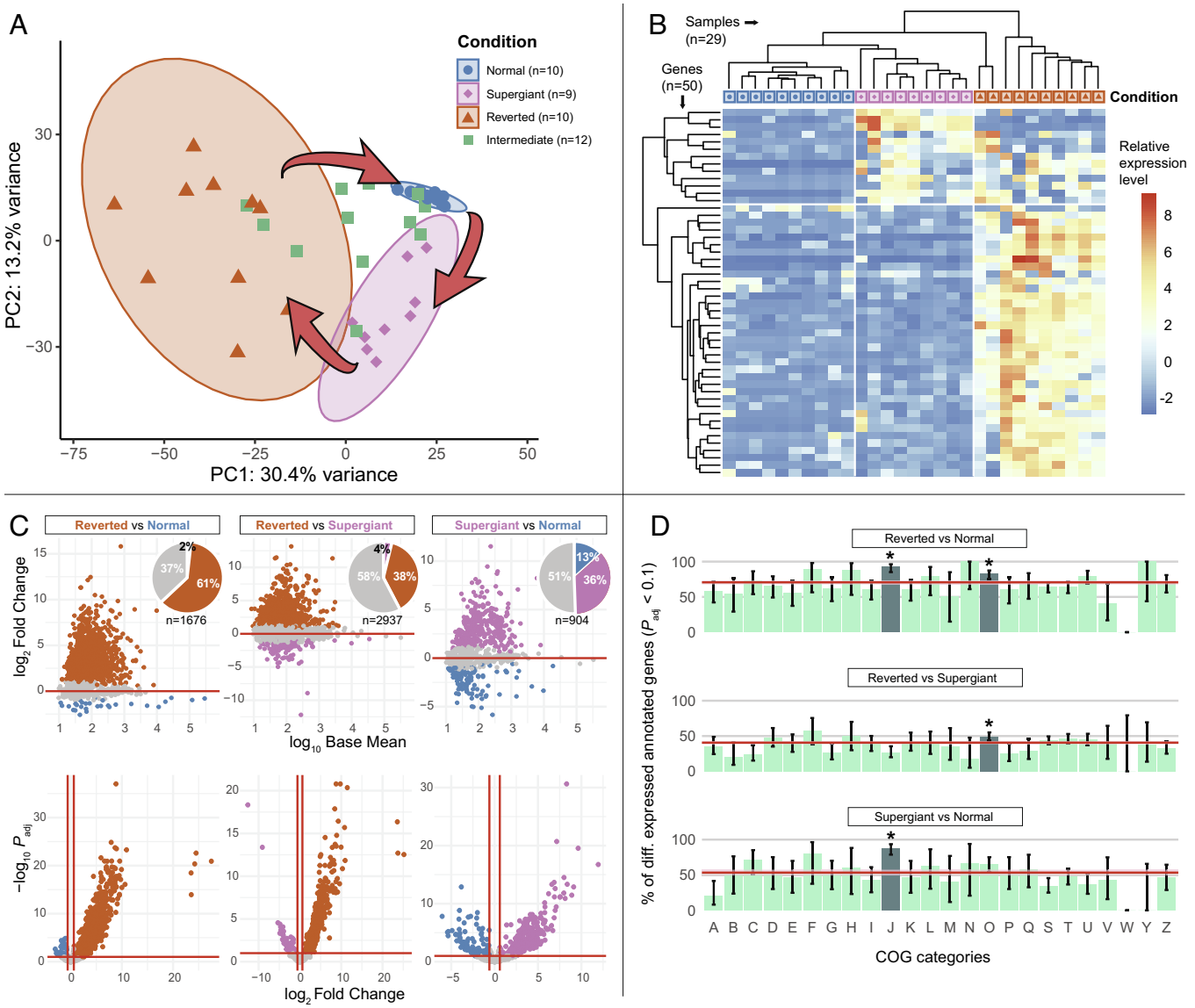

Fig. 4. The developmental cycle of *E. gigatrox* is reflected by changes in the expression profiles of two sets of protein-coding genes. (*A*) PC analysis of the top 500 genes in the rlog-transformed count matrix with the highest variance across samples: each dot corresponds to a different single-cell; 95% confidence ellipses highlight three distinct expression profiles corresponding to the three developmental conditions (data on cells displaying intermediate phenotypes is also reported). Arrows are used here to underline the inferred direction of the three-step regulatory cycle of *E. gigatrox*'s development. (*B*) Hierarchical clustering and heatmap on rlog-transformed count values displaying the 50 genes (rows) whose expression levels have the highest variance across samples (columns). Values represent their deviation from the gene's average across all samples. (*C*) Pair-wise differential expression analysis between three developmental conditions; each dot represents one protein-coding gene. MA-plots (*Top*): approximate posterior estimation for generalized linear model shrinkage estimator has been applied to reduce the noise associated with log Fold Changes expected from low count genes (48). *Bottom*: volcano plots. Datapoints in gray indicate genes which are not significantly differentially expressed ($P_{adj} > 0.1$ or $|\log_2 \text{Fold Change}| < 0.6$); datapoints in other colors indicate genes which are significantly upregulated in one developmental stage compared to the other. (*D*) Barplots showing the result of functional enrichment analyses: proportion of differentially expressed genes between each pair-wise comparison, which could be annotated within at least one COG functional category [following (49)]. Proportions of differentially expressed genes ($P_{adj} < 0.1$) calculated across all COG categories are represented by red lines. Genes involved in translation, ribosomal structure, and biogenesis (*J*), and posttranslational modification, protein turnover, and chaperones (O) are shown here as significantly enriched under certain conditions. P_{adj}= adjusted *P*-value.

To evaluate whether functional clusters of orthologous genes (COG) categories (49) were especially enriched in genes that are differentially expressed between developmental conditions, we compared the proportion of such genes across COG categories with that of the background for each condition pairing (Dataset S8). At least one of two COG categories always appeared to be enriched in differentially expressed (and annotated) genes (Fig. 4*D*): genes involved in translation, ribosomal structure, and biogenesis (J), and genes involved in posttranslational modification, protein turnover, and chaperones (O). Other COG categories showed no significant difference from the baseline.

GO-enriched terms were also identified among the annotated up- or down-regulated genes for each one of the three comparisons (Dataset S9 and *SI Appendix*, Figs. S5 and S6). Based on these results, we hypothesize a succession of major molecular events in the differentiation cycle of these cells. Specifically, normal cells actively regulate their plasma membrane composition homeostasis through TORC2 signaling, and they positively regulate MAP kinase activity, which typically involves response to a diverse array of stimuli. When cells differentiate into supergiants, these processes are downregulated. The typical membrane homeostasis is disrupted, perhaps allowing the cell to expand and change shape. At the same time, protein translation and energy consumption

are turned up, as suggested by higher ribosomal assembly activity and an enrichment in glycolytic process terms. Compared to the other stages, supergiants maintain a higher translation level and express genes involved in pathways linked to cell differentiation in multicellular organisms. Additionally, response to stress or some other stimulus is also significantly enriched. Once the cells revert, we hypothesize an upregulation of genes involved in mitotic cell cycle and in cyclin-dependent kinase activity. Because the protein repertoire that was produced in the supergiant stage is arguably no longer needed, autophagy and proteolysis ensue, while protein production subdues and MAP kinase activity regulation also returns to its normal active function. Cells that have recently reverted from supergiants still have relatively high translational levels, particularly higher production of proteins targeted to the ER lumen, and higher proteolytic activity, suggesting the existence of a fast protein turnover. Once back to normal, the expression levels linked to cyclin-dependent kinase (a cell cycle regulator) activity decrease, and so do translation and protein degradation levels. Finally, the TORC2-dependent homeostatic regulation of the plasma membrane, potentially involving vesicle retrograde trafficking, is set back into place.

Conclusions

Our results suggest a plausible hypothetical model for how and under which conditions the newly described ciliate, *E. gigatrox*, regulates the reversible development of supergiant cannibal cells. Under conditions where cells have access to enough small prey to sustain exponential growth, a stochastic switch that promotes initiation of supergiant differentiation is triggered at low frequencies. This baseline level of differentiation is an intriguing mystery, as is the exact mechanism of the switch, which should be further investigated. Upon transitioning to stationary phase, especially if there is low availability of small prey, the frequency of the switch increases, so that a small but detectable portion of the population activates the specialized developmental pathway, which may be stabilized by successful predation on a large prey item. There are performance tradeoffs in the change, explaining why the proportion of the committed cells is still small; it is likely a bet-hedging strategy (50). Supergiants change their trophic niche from filter-feeders to hunters exploiting larger prey, including genetically identical kin, by coordinating changes in their morphology and behavior. They are larger but clumsier, better hunters but worse swimmers. While the molecular details are still unclear, we hypothesize the process likely involves changes in cell cycle checkpoints, overall gene expression levels, and membrane homeostasis. Supergiants can persist and propagate themselves for variable periods of time, but a lack of large prey items or an abundance of small prey items promote dedifferentiation through uneven mitotic cycles and increased proteolytic activity. We can assume supergiant differentiation has costs, and a self-limiting feedback loop seems to have evolved: recently reverted cells maintain a unique gene expression profile that inhibits rapid redifferentiation, regardless of external conditions. This internal cool-down period might be adaptive, by postponing costly transitions at a time when the organism can reasonably expect favorable conditions to last for a while.

Testing this model and clarifying its molecular underpinnings represents a fascinating avenue for future experiments. While our transcriptomic analysis provides a starting point, more data will be needed to resolve significant differences between states, and even then, key regulatory proteins may escape detection and would require more direct investigation. Recent work involving molecular perturbations of cell patterning in other ciliates has uncovered intriguing connections between genes involved in animal development and cell patterning, suggesting great potential for discovery and even the possibility of general regulatory principles or mechanisms (51–55).

Inducible trophic polymorphism through morphological change occurs in diverse eukaryotic lineages including metazoans, amoebozoans, and other ciliates (56–60). In many cases, it is linked to diminishing resources (25, 56, 58, 59). More broadly, developmental phenotypic transitions are widespread across eukaryotic diversity, particularly in protists, and represent a means of dealing with environmental fluctuations when organisms do not have the ability to migrate to new, more favorable environments, as is the case for many animals. Also unlike in animals, the morphogenetic processes involved in unicellular protists must take place within a single plasma membrane and continuous cytosol, a topic about which little is known (17, 61). *E. gigatrox* is hence a case study at the interface between ecological and cytological questions, and this work provides a framework on which to build mechanistic studies to address both. By taking an integrative approach combining morphometric, behavioral, experimental, and molecular analysis, systems such as this can also be a foundation for a more general understanding of developmental processes in unicellular organisms, including their behavioral, ecological, and evolutionary implications. There are certainly many fascinating open questions. What internal and external cues induce supergiant induction and reversion? The transitions are regulated and linked to environmental conditions, but how cells actually sense abundance and prey type, or what specific external or internal signals respond to environmental conditions are all major unanswered questions. The current data suggest direct encounters with prey items play a role, but how an apparently stochastic developmental switch is regulated and how it is maintained over ecological and evolutionary timescales remain unclear. Similarly, large, raptorial cells have evolved multiple times in *Euplotes* and other lineages, raising questions about how they originate in natural contexts and under which conditions selection favors them over other strategies associated with low resource availability; reisolation and direct observation of cells in the field could help to address these questions. We have evidence that expression patterns are associated with specific stages, but the functional pathways remain untested, so how the modification of specific molecular processes might play a role in the evolutionary diversification of cellular form and function is yet to be determined. Importantly, the mechanisms by which cell geometry is rescaled and its detailed relationship to changes in cell behavioral capacities remain fascinating open questions. We hypothesize that supergiant formation and persistence involve heterochrony (62) stemming from activation of an alternative cell cycle. Extension, and perhaps repeated cycling of premitotic phases of the cell cycle could in principle account in part for increased cell size and cilia number in cirri observed in supergiants and would be reminiscent of the regulatory mechanism controlling multiciliated cell development in mammalian cells (63).

Although phenomena that are controlled by developmental mechanisms similar to those regulating supergiant formation are likely widespread among eukaryotes, their mechanistic bases, functional roles, and natural environmental contexts all must be better understood to clarify their ecological and evolutionary significance. *E. gigatrox* serves as a vivid illustration of unexplored diversity among protists and the potential this holds for shedding light into fundamental biological principles.

Materials and Methods

Initial Isolation and Sustained Culture of *E. gigatrox*. Cells were first collected by scraping filters for the water table system at CARMABI research station on the Caribbean island of Curaçao, which draws in seawater from a near-shore environment. Filter scrapings were deposited into vented cap T25 culture flasks (Corning, Corning, NY) and initially kept at room temperature for 2 wk before *Euplotes* cells were first directly observed. Cells were picked along with co-occurring bacteria and protists and placed into T25 culture flasks containing 10 mL of 10% Cereal Grass Media (CGM3; as in ref. 64) kept in a VWR Scientific model 2005 low temperature incubator at 22 °C. The ciliates were observed to proliferate under these conditions, and individual cells were then picked into T25 culture flasks with 10% CGM3 along with coisolated bacteria to establish strains E1 and E2 and incubated at 22 °C. Cell growth was monitored and after approximately 3 wk E1 and E2 were passaged at a 1:10 dilution into 10 mL of 25% CGM3 in T25 culture flasks and kept at 22 °C. Cultures were maintained under these conditions, with visual inspection and passaging approximately every 2 to 3 wk. Supergiants were observed sporadically during this time. While E2 played a role in initial observations, a coisolated amoeba contributed to less reliable *Euplotes* growth by also feeding on prey bacteria, and therefore strain E1 was used for subsequent experimental work.

For sustained, long-term culture of strain E1, cells were transferred to 15% red algae stock media (RA; as in ref. 65). Cultures were maintained in T25 flasks at ambient room temperature conditions covered loosely by plastic wrap to reduce evaporation. Cells were passaged approximately every 2 wk at a 2:10 dilution into 10 mL fresh media. Under these culture conditions, supergiants were reliably observed.

Light Microscopy and Morphometric Analysis. Cells for morphometric analysis were imaged in Fluorodishes (World Precision Instruments FD35-100, Sarasota, FL) by differential interference contrast microscopy using a 20× Plan Apochromat Lambda D (0.8 NA) Nikon objective on a Nikon ECLIPSE Ti2 inverted microscope (Nikon, Shinagawa, Tokyo, Japan) with a Photometrics Kinetix camera (Teledyne, Waterloo, ON, Canada). Cell measurements were performed manually in Fiji (66).

For routine observation and documentation (e.g., Fig. 1 *B* and *L*), cells were imaged in T25 culture flasks by brightfield or phase contrast using a 20× Plan Fluor ELWD (0.45 NA) Nikon objective on a Nikon ECLIPSE Ts2 inverted microscope with a Nikon Z6 camera.

Scanning Electron Microscopy. Cells were deposited onto plasma-cleaned coverslips (#1.5, 12 mm, Electron Microscopy Sciences, 72290-04, Hatfield, PA) coated with poly-D-lysine (Sigma Aldrich P6407-5MG, Burlington, MA) and fixed for 2 h at 4 °C in 4% paraformaldehyde and 2.5% glutaraldehyde in PHEM buffer and artificial seawater (ASW, ASTM D 1141, Ricca Chemical Company, 8363-5, Arlington, TX). Samples were then rinsed with fresh water and then dehydrated by ethanol dilution series according to the following steps: 25% ETOH in water (5 min), 50% ETOH (5 min), 75% ETOH (5 min followed by overnight incubation at 4 °C), 95% ETOH, 100% ETOH (10 min, repeated for a total of three times). Samples were critical point dried for 80 min using a Leica EM CPD300 (Leica Microsystems, Wetzlar, Germany) under a slow automated setting and sputter coated with 6 nm of iridium using a Leica EM ACE600 before imaging using a Phenom Pharos G2 desktop field emission gun scanning electron microscope (Thermo Scientific, Waltham, MA).

Phylogenetic Analysis. The full-length SSU rRNA sequence was extracted from the reference transcriptome (see below) and confirmed to be identical to a sequence of the SSU rRNA gene obtained through DNA extraction and PCR. It was aligned with 77 representative orthologs from other *Euplotes* species collected from GenBank as well as 11 sequences from related genera (to serve as outgroup) using the linsi option in mafft (67) v7.520. The alignment was trimmed at both ends to remove sites with more than 50% missing data, resulting in an 89 taxa by 2,168 sites character matrix. Maximum likelihood phylogenetic inference was performed on IQ-TREE (68) v2.2.2.7, using the GTR+F + I + G4 model as suggested by all information criteria, and running 1,000 nonparametric bootstrap pseudoreplicates for support.

Cell Motility Analysis. For motility analysis, 2 mL of cell culture were taken directly from culture flasks and placed in fluorodishes. This amount of fluid ensured sufficient depth to allow unconstrained swimming behavior. Cells were imaged in dark field on a Zeiss Axio Zoom.V16 microscope with a Zeiss 1.0× Plan Neo Fluor objective (NA 0.25) and a Zeiss AxioCam 305 color camera (Zeiss Microscopy, Oberkochen, Germany). Videos were acquired at 60 frames/s and were preprocessed in Fiji by first subtracting the individual average pixel value over the entire video (background) from each video frame and then smoothed by applying a median filter with a 4-pixel radius. Tracking was then performed with the TrackMate Fiji plugin (69, 70) using the following settings: threshold detector for blob detection, LAP tracker frame to frame linking = 10 px, gap closing = 10 px, and frame gap = 10 frames. To remove misidentified tracks, a postprocessing filter for tracks less than 40 frames and speeds greater than 16 px/frame was applied. Supergiants were discriminated from normal morphs based on size by applying a postprocessing filter with a threshold radius of 7 pixels, where blobs above this size were designated supergiants and those below were designated normal morphs. Visual inspection confirmed that this threshold never led to the misidentification of supergiants. Trajectories were then smoothed using a Savitzky–Golay filter with polynomial order 2 and frame length 5 implemented using the sgolay function in Matlab (R2023b, Mathworks, Natick, MA). Instantaneous speeds were calculated at discrete time t as $v(t) = \frac{\sqrt{(x_t - x_{t-1})^2 + (y_t - y_{t-1})^2}}{dt}$ where (x_i, y_i) are the coordinates at frame i and dt is the interframe time interval. Turning angles along trajectories were calculated by $\theta = atan2\left(|\vec{p} \times \vec{q}|, \vec{p} \cdot \vec{q}\right)$ where $\vec{p} = \vec{r}_t - \vec{r}_{t-5}$ and $\vec{q} = \vec{r}_{t+5} - \vec{r}_t$ are vectors approximately tangent to adjacent positions along the trajectory where $\vec{r}_n$ denotes a cell position at frame n, following [15]. MSD was calculated by $\mathrm{MSD}(\tau) = \frac{1}{T-\tau} \sum_{i=1}^{T-\tau} \left(\vec{r}_{i+\tau} - \vec{r}_i\right)^2, i = 1, \ldots, T$ for time lag τ, incremented by the frame rate, where T is the time for the final frame of the trajectory. MSDs were normalized by dividing by the value at the first point of the MSD curve. 95% CI were determined by bootstrapping using the bootci function in Matlab with 1,000 samples.

For swimming comparison experiments, cells were gently displaced from the coverslip surface of fluorodishes by gentle shaking of the dish or pipette aspiration while simultaneously recording on the Axio Zoom microscope (setup detailed above). Tracking was performed in TrackMate as described above, and each trajectory of a swimming cell was manually evaluated to determine the beginning and end of unconstrained swimming, free of apparent influence by fluid currents introduced by knocking cells from the coverslip.

Supergiant Induction Experiments and Analysis. All supergiant induction experiments presented in the main text (Fig. 3 *A*, *B*, and *E*) were conducted in 24-well plates (Fisher Scientific 09-761-146) in 2 mL growth media or ASW. For experiments reported in Fig. 3*A*, 10 normal morph cells were picked from a culture 1 wk after a fresh passage, placed into each well, and allowed to proliferate at room temperature. Plates were sealed with two layers of parafilm to reduce evaporation. Cell counts were performed manually, by dividing wells into quadrants for normal morphs, and directly for supergiants; the average of three counts was taken. Cell counts were performed using a Zeiss Stemi 508 Microscope under darkfield illumination. For experiments reported in Fig. 3*B*, individual normal morph or supergiant cells were picked into individual wells, and plates were monitored every day for the presence of supergiants. See *SI Appendix*, Table S1 for methodological information on additional supergiant induction experiments not reported in main text figures.

Single-Cell Collection for Transcriptomics. Supergiant cells were transferred with a pulled glass micropipette under a Zeiss Stemi 508 Microscope into separate wells of a glass spot plate with depressions, in autoclaved filtered seawater and with no food source. Cell division and consequent reversion to normal morphs were monitored by checking the wells every 2 h four times. After ~24 h, when all cells had reverted to the normal phenotype, 10 of them were individually collected, washed in sterile medium to further reduce contamination, and placed each into a 0.2 mL tube containing 2 μL of lysis buffer (71, 72). Additionally, 10 normal and 9 supergiant cells were individually collected from the original cultures and also placed in lysis buffer. Finally, 12 cells with intermediate or ambiguous features were also collected and isolated, 6 from each of two separate cultures of the same clonal strain. The 41 collected cells were stored at −70 °C until further use.

RNA-seq, Reference Transcriptome Coassembly, and Contamination Removal. First, frozen samples were subjected to at least four freeze–thaw cycles to facilitate cell lysis (73). Then, cDNA was extracted from each sample and purified following the Smart-seq2 protocol (72). The obtained cDNA yield was quantified with Qubit™ dsDNA HS Assay Kit and fluorometer (Thermo Fisher Scientific). The cDNA samples were submitted to the Sequencing + Bioinformatics Consortium of the University of British Columbia (BC, Canada). There, length composition and quality of the samples were assessed with an Agilent Bioanalyzer (High Sensitivity DNA Assay); libraries were prepared for sequencing using Illumina DNA Prep; paired-end sequencing was carried out on a NextSeq 500 platform (2 × 150 bp).

Prior to assembly, all reads were preprocessed with Trimmomatic (74) v0.39 to remove adapters and for quality filtering. Then, rnaSPAdes (75) v3.15.5 was used to coassemble reads from all samples into one preliminary transcriptome, as an initial step toward constructing a comprehensive reference. An initial set of 57,651 transcripts (each longer than 300 bp) and total length of 56.8 Mbp was obtained from which coding regions were predicted through TransDecoder v5.5.0 with homology searches (76); the "Euplotid" genetic code was selected, which differs from the universal genetic code as it replaces the UGA codon's stop signal with a cytosine (77). The predicted coding sequences were clustered with cd-hit-est (78) setting a lower threshold of 90% identity, to reduce redundancy and limit the chance of multiple mapping during the alignment of the reads to the reference transcriptome. The aminoacidic sequences were blasted with BLASTp to identify the likely source of each transcript and limit any potential contamination: all transcripts hitting Alveolata were kept; other sequences with less than 80% identity were kept if their GC content ranged within the 10th and the 90th percentile of the Alveolata distribution (36% and 42% respectively). All hits to Metazoa, Fungi, Stramenopila, Viridiplantae, *Pseudomonadota*, *Terrabacteria*, *Bacteroidota*, *Planctomycetota*, and viruses were filtered out. After sequences were clustered and potential sources of contamination were removed, the final reference transcriptome retained 35,567 transcripts and had a total length of 38.3 Mbp, corresponding to 27,557 protein-coding genes. Busco (79) v5.4.3 and its "alveolata_odb10" database (n = 171) were used to estimate and compare the completeness and the level of duplication of the initial and final reference transcriptome. While the BUSCO completeness score expectedly decreased from 71.3 to 57.9% throughout the filtering process, the proportion of single-copy markers increased from 45.6 to 56.1%, and that of duplicated markers plummeted from 25.7 to 1.8%, thus improving univocal read alignment to the reference. The proportions of fragmented matches remained roughly unchanged (18.7% and 19.3% respectively).

Transcriptomics—Data Analyses in R. All analyses were conducted on R v4.2.1/4.3.2/4.5.2. Transcript quantification into count matrices, gene-level exploratory analysis and visualization, and differential expression analyses were carried out using the Bioconductor (80) v3 R packages and guidelines described by ref. 81, with few adjustments. Briefly, reads from each sample were separately aligned to the reference transcriptome using bowtie (82) v2.5.3; gene models were defined from the GFF3 file obtained from the TransDecoder coding region prediction described earlier; sample information was added to a *SummarizedExperiment* (SE) object, choosing a developmental condition as reference level; the SE object was then converted into a *DESeqDataSet* (dds) object (count matrix) for further analysis. The dataset was then prefiltered keeping only rows that have a count of at least 10 for a minimal number of samples. The regularized-logarithm (rlog) transformation was applied to make the data homoscedastic for successive exploratory analyses.

Transcriptomics—Exploratory Analyses. From the rlog-transformed count matrix, the 500 genes with the highest variance across samples were selected for a PCA, performed through the built-in R function *prcomp()*. The *PCAtest* package (47) v0.0.1 was used to test the PCA overall significance, that of each PC, and that of the correlation of gene variables to the PCs based on 1,000 bootstrap replicates and 1,000 random permutations. The minimum number of significant PCs to retain was further assessed through Horn's parallel analysis (83) implemented within the *paran* v1.5.3 package (84) using 10,000 iterations. Among the six retained PCs, the first two combined covered a large fraction of the total variance (43.6%), so they were selected to plot their score values using ggplot2 v3.5.0 from the tidyverse R collection (85). The clustering patterns of the data points and their significance were evaluated with an analysis of similarity (ANOSIM) test implemented with the *vegan* v2.6-4 package (86), setting 999 unrestricted permutations: six tests were performed for each pair-wise comparison between the examined groups (normal, supergiant, reverted, intermediate); for each, a distance matrix was calculated based on Euclidean distances between the data points; *R* statistics and their respective *P*-values were then obtained for each pair. To correct for the increase of the type I error rate due to multiple testing, *P*-values were adjusted using the Bonferroni correction. To measure the clustering tendency of data points as a whole, the ANOSIM test was also performed across all groups.

The top 50 and the top 500 genes of the rlog-transformed count matrix with the highest variance across samples were selected for hierarchical clustering to identify patterns of expression (if present) between the different developmental conditions. Data from the intermediate-looking cells were disregarded from this and further analyses, because of their lack of unambiguous characterization. The clustering was carried out using pheatmap (87) with the default clustering method (i.e., complete linkage).

Pair-Wise Differential Gene Expression Analyses. Differences in the expression levels between developmental conditions of *Euplotes* were examined individually by pair-wise comparison through DESeq2 (88) v1.36.0. Precautions were adopted in dealing with potential zero-inflation effects expected in single-cell datasets (89). For this, the DESeq2 manual recommendations (90) for single-cell analysis were followed: size factors were calculated using the *scran* package; the Wald test was replaced with the likelihood ratio test for significance testing; other *DESeq()* arguments were adjusted as: useT = TRUE, minmu = 1e-6, and minReplicatesForReplace = Inf.

Functional Annotation and Enrichment Analyses. Genes predicted from the reference transcriptome were annotated using eggNOG-mapper (91) v2.1.0-1 with the eggNOG database (92) v5.0.2. The search step of eggNOG-mapper relies on DIAMOND (93) v2.0.15. Domain-scale annotations were obtained with InterProScan (94, 95) v5.75 by running all the default analyses. The eggNOG-mapper annotation output for each gene was matched with the results obtained from the differential expression analyses; then, proportions of differentially expressed genes with an adjusted *P*-value < 0.1 were calculated for each cluster of orthologous group (COG) functional category and across all categories. CI for each proportion were obtained using the Wilson score interval (96).

EggNOG-mapper and InterProScan GO term annotations were integrated to compile a de novo organism database using makeOrgPackage() with AnnotationForge v1.52.0 (97). The resulting database contained an average of 30.36 GO terms/gene. GO ontology information was added from GO.db v3.22 (98). TopGO v2.62.0 (99) was used for GO term enrichment analyses based on the "Biological Processes" GO ontology. Groups of down- and up-regulated genes were defined from each of the three pair-wise comparisons based on the following criteria: adjusted *P*-value < 0.05 and $|\log_2 \text{Fold Change}| > 0.6$. A topGO data object was generated for each one of the six groups of differentially expressed genes, then runTest() was used to test the significance of the GO terms in each group with a weighted Fisher test (algorithm = weight01). In each group of most significantly enriched GO terms, the top 100 with *P*-value < 0.05 (Dataset S9) were carried over and grouped based on their semantic similarity, calculated using the calculateSimMatrix() function with the "Relevance" method within rrvgo v1.22.0 (100). From the same R package, reduceSimMatrix() was used to reduce the GO terms and group them based on a semantic similarity threshold of 0.9. Scatterplots and treemaps (*SI Appendix*, Figs. S5 and S6) were generated with rrvgo functions scatterPlot() and treemapPlot() respectively.

Data, Materials, and Software Availability. Image data have been deposited in figshare (101). All other data are included in the manuscript and/or supporting information.

ACKNOWLEDGMENTS. We would like to thank David Booth for the use of his light microscopes and Dyche Mullins for the use of his electron microscope, sputter coater, and critical point dryer. We would also like to thank Kristen Marhaver for giving us access to the filters from which *E. gigatrox* was isolated. Thanks to Vojtěch Žárský for providing initial guidance and technical support in processing transcriptomic data for the analysis of gene differential expression. B.T.L. would like to acknowledge funding from the Merck Fellowship of the Jane Coffin Childs Memorial Fund for Biomedical Research and startup funds from the RPI Department of Biological Sciences. B.T.L. also thanks Nicole King and Wallace Marshall for tolerating the existence of the initial

project that eventually led to this publication and for harboring cell cultures in their labs. P.J.K. acknowledges funding from the Gordon and Betty Moore Foundation (https://doi.org/10.37807/GBMF9201). D.G. thanks the University of British Columbia for funding this research through the Four Year Doctoral Fellowship Award.

Author affiliations: [a]Department of Biological Sciences, Center for Biotechnology and Interdisciplinary Studies, and Darrin Freshwater Institute, Rensselaer Polytechnic Institute, Troy, NY 12180; [b]Department of Botany, University of British Columbia, Vancouver, BC V6T 1Z4, Canada; and [c]Department of Cellular and Molecular Pharmacology and HHMI, University of California, San Francisco, CA 94143

1. F. Burki, A. J. Roger, M. W. Brown, A. G. B. Simpson, The new tree of eukaryotes. *Trends Ecol. Evol.* **35**, P43–P55 (2020).
2. P. J. Keeling, Combining morphology, behaviour and genomics to understand the evolution and ecology of microbial eukaryotes. *Philos. Trans. R. Soc. Lond. B Biol. Sci.* **374**, 20190085 (2019).
3. B. T. Larson, Perspectives on principles of cellular behavior from the biophysics of protists. *Integr. Comp. Biol.* **63**, 1405–1421 (2023).
4. T. Brunet, N. King, The origin of animal multicellularity and cell differentiation. *Dev. Cell* **43**, 124–140 (2017).
5. F. Burki, M. M. Sandin, M. Jamy, Diversity and ecology of protists revealed by metabarcoding. *Curr. Biol.* **31**, R1267–R1280 (2021).
6. C. Y. Cheng, E. Orias, J. Y. Leu, A. P. Turkewitz, The evolution of germ–soma nuclear differentiation in eukaryotic unicells. *Curr. Biol.* **30**, R502–R510 (2020).
7. C. W. Greider, E. H. Blackburn, A telomeric sequence in the RNA of *Tetrahymena* telomerase required for telomere repeat synthesis. *Nature* **337**, 331–337 (1989).
8. T. M. Bryan, J. M. Sperger, K. B. Chapman, T. R. Cech, Telomerase reverse transcriptase genes identified in *Tetrahymena thermophila* and *Oxytricha trifallax*. *Proc. Natl. Acad. Sci. U.S.A.* **95**, 8479–8484 (1998).
9. D. P. Singh *et al.*, Genome-defence small RNAs exapted for epigenetic mating-type inheritance. *Nature* **509**, 447–452 (2014).
10. H. Onsbring, M. Jamy, T. J. G. Ettema, RNA sequencing of *Stentor* cell fragments reveals transcriptional changes during cellular regeneration. *Curr. Biol.* **28**, 1281–1288 (2018).
11. E. Flaum, E. M. Prakash, Curved crease origami and topological singularities enable hyperextensibility of *L. olor*. *Science* **384**, eadk5511 (2024).
12. G. Di Giuseppe *et al.*, Antarctic and Arctic populations of the ciliate *Euplotes nobilii* show common pheromone-mediated cell-cell signaling and cross-mating. *Proc. Natl. Acad. Sci. U.S.A.* **108**, 3181–3186 (2011).
13. V. Boscaro *et al.*, Parallel genome reduction in symbionts descended from closely related free-living bacteria. *Nat. Ecol. Evol.* **1**, 1160–1167 (2017).
14. B. T. Larson, J. Garbus, J. B. Pollack, W. F. Marshall, A unicellular walker controlled by a microtubule-based finite-state machine. *Curr. Biol.* **32**, 3745–3757 (2022).
15. H. Laeverenz-Schlogelhofer, K. Y. Wan, Bioelectric control of locomotor gaits in the walking ciliate Euplotes. *Curr. Biol.* **34**, 697–709 (2024).
16. B. N. Wise, The morphogenetic cycle in *Euplotes eurystomus* and its bearing on problems of ciliate morphogenesis. *J. Protozool.* **12**, 626–648 (1965).
17. J. Frankel, *Pattern Formation: Ciliate Studies and Models* (Oxford University Press, New York, NY, 1989).
18. K. J. Aufderheide, J. Frankel, N. E. Williams, Formation and positioning of surface-related structures in protozoa. *Microbiol. Rev.* **44**, 252–302 (1980).
19. M. D. Ruehle, S. Li, D. A. Agard, C. G. Pearson, Poc1 bridges basal body inner junctions to promote triplet microtubule integrity and connections. *J. Cell Biol.* **223**, e202311104 (2024).
20. J. A. Dawson, Cannibalism in a ciliate, *Blepharisma*. *Proc. Soc. Exp. Biol. Med.* **26**, 335–336 (1929).
21. N. Ricci, D. C. Riggio, Cannibals of *Oxytricha bifaria* (Ciliata, Hypotrichida): I. A crowding-dependent cell differentiation. *J. Exp. Zool.* **229**, 339–347 (1984).
22. M. Tuffrau, G. Fryd-Versavel, H. Tuffrau, J. Génermont, Description of *Euplotes versatilis* n. sp., a marine tropical ciliate exhibiting an unusually extensive phenotypic plasticity. *Eur. J. Protistol.* **36**, 355–366 (2000).
23. A. Banerji, P. J. Morin, Phenotypic plasticity, intraguild predation and anti-cannibal defences in an enigmatic polymorphic ciliate. *Funct. Ecol.* **23**, 427–434 (2009).
24. A. Omar, S. W. Jang, J.-H. Jung, Polymorphism, gigantism, and cannibalism, one stylonychid ciliate (Ciliophora, Hypotricha) to rule them all. *Front. Microbiol.* **14**, 1159634 (2023).
25. J. A. Dawson, An experimental study of an amicronucleate *Oxytricha*. *J. Exp. Zool.* **29**, 473–513 (1919).
26. J. Kusch, Predator-induced morphological changes in *Euplotes* (Ciliata): Isolation of the inducing substance released from *Stenostomum sphagnetorum* (Turbellaria). *J. Exp. Zool.* **265**, 613–618 (1993).
27. S. L. Duquette, R. Altwegg, B. R. Anholt, Factors affecting the expression of inducible defences in *Euplotes*: Genotype, predator density and experience. *Funct. Ecol.* **19**, 648–655 (2005).
28. N. Ricci, R. Giannetti, C. Miceli, The ethogram of *Euplotes crassus* (Ciliata, Hypotrichida): I. The wild type. *Eur. J. Protistol.* **23**, 129–140 (1988).
29. M. J. Saxton, K. Jacobson, Single-particle tracking: Applications to membrane dynamics. *Annu. Rev. Biophys. Biomol. Struct.* **26**, 373–399 (1997).
30. G. Volpe, G. Volpe, The topography of the environment alters the optimal search strategy for active particles. *Proc. Natl. Acad. Sci. U.S.A.* **114**, 11350–11355 (2017).
31. O. Berger-Tal, S. Bar-David, Recursive movement patterns: Review and synthesis across species. *Ecosphere* **6**, 1–12 (2015).
32. T. Narazaki *et al.*, Similar circling movements observed across marine megafauna taxa.. *iScience* **24**, 102221 (2021).
33. E. E. Nuzhin, M. E. Panov, N. V. Brilliantov, Why animals swirl and how they group. *Sci. Rep.* **11**, 20843 (2021).
34. S. Tokunaga *et al.*, Autonomous spiral motion by a small-type robot on an obstacle-available surface. *Micromachines* **12**, 375 (2021).
35. M. Müller, R. Wehner, The hidden spiral: Systematic search and path integration in desert ants, *Cataglyphis fortis*. *J. Comp. Physiol. A* **175**, 525–530 (1994).
36. M. G. Fricke, J. P. Hecker, A. D. Griego, L. T. Tran, M. E. A. Moses, "A distributed deterministic spiral search algorithm for swarms" in *IEEE/RSJ International Conference on Intelligent Robots and Systems*, G. K. H. Zupanc, Ed. (IEEE, 2019), pp. 4430–4436.
37. L. J. Galindo, T. A. Richards, J. A. Nirody, Evolutionarily diverse fungal zoospores show contrasting swimming patterns specific to ultrastructure. *Curr. Biol.* **34**, 4567–4576 (2024).
38. T. Fenchel, Orientation in two dimensions: Chemosensory motile behaviour of *Euplotes vannus*. *Eur. J. Protistol.* **40**, 49–55 (2004).
39. E. M. Nelsen, Transformation in *Tetrahymena thermophila*: Development of an inducible phenotype. *Dev. Biol.* **66**, 17–31 (1978).
40. D. H. Lynn, *The Ciliated Protozoa: Characterization, Classification, and Guide to the Literature* (Springer, New York, NY, ed. 3, 2008).
41. M. J. Dayel *et al.*, Cell differentiation and morphogenesis in the colony-forming choanoflagellate *Salpingoeca rosetta*. *Dev. Biol.* **375**, 73–82 (2011).
42. J. Kusch, K. Heckmann, Isolation of the Lembadion-factor, a morphogenetically active signal, that induces *Euplotes* cells to change from their ovoid form into a larger lateral winged morph. *Dev. Genet.* **13**, 241–246 (1992).
43. R. Altwegg, K. B. Marchinko, S. L. Duquette, B. R. Anholt, Dynamics of an inducible defence in the protist *Euplotes*. *Arch. Hydrobiol.* **160**, 431–446 (2004).
44. F.-M. Möller, S. Flöder, G. Di Giuseppe, S. Devi Moorthi, Resource supply and intraspecific variation in inducible defense determine predator-prey interactions in an intraguild predation food web. *Eur. J. Protistol.* **95**, 126114 (2024).
45. R.A. Alegado *et al.*, A bacterial sulfonolipid triggers multicellular development in the closest living relatives of animals. *eLife* **1**, e00013 (2012).
46. O. N. Perotti, G. Viramontes-Esparza, D. S. Booth, A red algal polysaccharide influences the multicellular development of the choanoflagellate *Salpingoeca rosetta*. *Curr. Biol.* **35**, 3767–3776 (2025).
47. A. Camargo, PCAtest: Testing the statistical significance of principal component analysis in R. *PeerJ* **10**, e12967 (2022).
48. A. Zhu, J. G. Ibrahim, M. I. Love, Heavy-tailed prior distributions for sequence count data: Removing the noise and preserving large differences. *Bioinformatics* **35**, 2084–2092 (2019).
49. R. L. Tatusov *et al.*, The COG database: An updated version includes eukaryotes. *BMC Bioinformatics* **4**, 41 (2003).
50. D. Cohen, Optimizing reproduction in a randomly varying environment. *J. Theor. Biol.* **16**, 1–14 (1967).
51. C. G. Pearson, M. Winey, Basal body assembly in ciliates: The power of numbers. *Traffic* **10**, 461–471 (2009).
52. L. Tavares *et al.*, Mob1: Defining cell polarity for proper cell division. *J. Cell Sci.* **125**, 516–527 (2012).
53. N. Galati *et al.*, DisAp-dependent striated fiber elongation is required to organize ciliary arrays. *J. Cell Biol.* **207**, 705–715 (2014).
54. M. M. Slabodnick *et al.*, The kinase regulator Mob1 acts as a patterning protein for *Stentor* morphogenesis. *PLoS Biol.* **12**, e1001861 (2013).
55. C. Yan *et al.*, Spatiotemporal control of cortical centrin patterning by regionalized Sfi1 family scaffolding proteins in *Stentor coeruleus*. bioRxiv [Preprint] (2025). https://doi.org/10.1101/2025.08.11.669701(Accessed 15 August 2025).
56. N. E. Williams, Polymorphism in *Tetrahymena vorax*. *J. Protozool.* **8**, 403–410 (1961).
57. G. A. Polis, The evolution and dynamics of intraspecific predation. *Annu. Rev. Ecol. Syst.* **12**, 225–251 (1981).
58. L. V. Pomeroy, "Developmental polymorphism in the tadpoles of the spadefoot toad *Scaphiopus multiplicatus*," PhD Dissertation, University of California, Riverside, CA (1981).
59. K. E. Lewis, D. H. O'Day, The regulation of sexual development in *Dictyostelium discoideum*: Cannibalistic behaviour of the giant cell. *Can. J. Microb.* **31**, 423–428 (1985).
60. S. Fais, Cannibalism: A way to feed on metastatic tumors. *Cancer Lett.* **258**, 155–164 (2007).
61. W. F. Marshall, Pattern formation and complexity in single cells. *Curr. Biol.* **30**, R544–R552 (2020).
62. K. J. McNamara, Heterochrony: The evolution of development. *Evol. Educ. Outreach* **5**, 203–218 (2012).
63. S. P. Choksi *et al.*, An alternative cell cycle coordinates multiciliated cell differentiation. *Nature* **630**, 214–221 (2024).
64. B. T. Larson *et al.*, Biophysical principles of choanoflagellate self-organization. *Proc. Natl. Acad. Sci. U.S.A.* **117**, 1303–1311 (2020).
65. O. N. Perotti, G. Viramontes-Esparza, D. S. Booth, A red algal polysaccharide influences the multicellular development of the choanoflagellate *Salpingoeca rosetta*. *Curr. Biol.* **35**, 3757–3776 (2025).
66. J. Schindelin *et al.*, Fiji: An open-source platform for biological-image analysis. *Nat. Methods* **9**, 676–682 (2012).
67. K. Katoh, D. M. Standley, MAFFT multiple sequence alignment software version 7: Improvements in performance and usability. *Mol. Biol. Evol.* **30**, 772–780 (2013).
68. B. Q. Minh *et al.*, IQ-TREE 2: New models and efficient methods for phylogenetic inference in the genomic era. *Mol. Biol. Evol.* **37**, 1530–1534 (2020).
69. J.-Y. Tinevez *et al.*, TrackMate: An open and extensible platform for single-particle tracking. *Methods* **115**, 80–90 (2017).
70. D. Ershov *et al.*, TrackMate 7: Integrating state-of-the-art segmentation algorithms into tracking pipelines. *Nat. Methods* **19**, 829–832 (2022).
71. M. Kolisko, V. Boscaro, F. Burki, D. H. Lynn, P. J. Keeling, Single-cell transcriptomics for microbial eukaryotes. *Curr. Biol.* **24**, R1081–R1082 (2014).
72. S. Picelli *et al.*, Full-length RNA-seq from single cells using Smart-seq2. *Nat. Protoc.* **9**, 171–181 (2014).
73. H. Onsbring *et al.*, An efficient single-cell transcriptomics workflow for microbial eukaryotes benchmarked on *Giardia intestinalis* cells. *BMC Genomics* **21**, 448 (2020).
74. A. M. Bolger, M. Lohse, B. Usadel, Trimmomatic: A flexible trimmer for Illumina sequence data. *Bioinformatics* **30**, 2114–2120 (2014).
75. E. Bushmanova, D. Antipov, A. Lapidus, A. D. Prjibelski, rnaSPAdes: A de novo transcriptome assembler and its application to RNA-Seq data. *Gigascience* **8**, giz100 (2019).

76. B. Haas *et al.*, De novo transcript sequence reconstruction from RNA-seq using the Trinity platform for reference generation and analysis. *Nat. Protoc.* **8**, 1494–1512 (2013).
77. F. Meyer *et al.*, UGA is translated as cysteine in pheromone 3 of *Euplotes octocarinatus*. *Proc. Natl. Acad. Sci. U.S.A.* **88**, 3758–3761 (1991).
78. L. Fu, B. Niu, Z. Zhu, S. Wu, W. Li, CD-HIT: Accelerated for clustering the next-generation sequencing data. *Bioinformatics* **28**, 3150–3152 (2012).
79. M. Manni, M. R. Berkeley, M. Seppey, F. A. Simão, E. M. Zdobnov, BUSCO update: Novel and streamlined workflows along with broader and deeper phylogenetic coverage for scoring of eukaryotic, prokaryotic, and viral genomes. *Mol. Biol. Evol.* **38**, 4647–4654 (2021).
80. W. Huber *et al.*, Orchestrating high-throughput genomic analysis with Bioconductor. *Nat. Methods* **12**, 115–121 (2015).
81. M. I. Love, S. Anders, V. Kim, W. Huber, RNA-Seq workflow: Gene-level exploratory analysis and differential expression. *F1000Res.* **4**, 1070 (2015).
82. B. Langmead, S. L. Salzberg, Fast gapped-read alignment with Bowtie 2. *Nat. Methods* **9**, 357–359 (2012).
83. J. L. Horn, A rationale and test for the number of factors in factor analysis. *Psychometrika* **30**, 179–185 (1965).
84. A. Dinno, Implementing Horn's parallel analysis for principal component analysis and factor analysis. *Stata J.* **9**, 291–298 (2009).
85. H. Wickham *et al.*, Welcome to the Tidyverse. *J. Open Source Softw.* **4**, 1686 (2019).
86. J. Oksanen *et al.*, vegan: Community Ecology Package (R package version 2.6-4, CRAN, 2022). https://CRAN.R-project.org/package=vegan.
87. R. Kolde, pheatmap: Pretty Heatmaps (R package version 1.0.12, CRAN, 2019). https://CRAN.R-project.org/package=pheatmap.
88. M. I. Love, W. Huber, S. Anders, Moderated estimation of fold change and dispersion for RNA-seq data with DESeq2. *Genome Biol.* **19**, 24 (2018).
89. K. Van den Berge *et al.*, Observation weights unlock bulk RNA-seq tools for zero inflation and single-cell applications. *Genome Biol.* **15**, 550 (2014).
90. M. Love, S. Anders, W. Huber, Analyzing RNA-seq data with DESeq2. https://bioconductor.org/packages/devel/bioc/vignettes/DESeq2/inst/doc/DESeq2.html. Accessed 12 March 2024.
91. C. P. Cantalapiedra, A. Hernández-Plaza, I. Letunic, P. Bork, J. Huerta-Cepas, eggNOG-mapper v2: Functional annotation, orthology assignments, and domain prediction at the metagenomic scale. *Mol. Biol. Evol.* **38**, 5825–5829 (2021).
92. J. Huerta-Cepas *et al.*, eggNOG 5.0: A hierarchical, functionally and phylogenetically annotated orthology resource based on 5090 organisms and 2502 viruses. *Nucleic Acids Res.* **47**, D309–D314 (2019).
93. B. Buchfink, K. Reuter, H. G. Drost, Sensitive protein alignments at tree-of-life scale using DIAMOND. *Nat. Methods* **18**, 366–368 (2021).
94. P. Jones *et al.*, InterProScan 5: Genome-scale protein function classification. *Bioinformatics* **30**, 1236–1240 (2014).
95. M. Blum *et al.*, The InterPro protein families and domains database: 20 years on. *Nucleic Acids Res.* **49**, D344–D354 (2021).
96. E. B. Wilson, Probable inference, the law of succession, and statistical inference. *J. Am. Stat. Assoc.* **22**, 209–212 (1927).
97. M. Carlson, H. Pagès, AnnotationForge: Tools for building SQLite-based annotation data packages (R package version 1.52.0, Bioconductor, 2025). https://bioconductor.org/packages/AnnotationForge.
98. M. Carlson, GO.db: A set of annotation maps describing the entire Gene Ontology (R package version 3.22.0, Bioconductor, 2025).
99. A. Alexa, J. Rahnenführer, topGO: Enrichment analysis for Gene Ontology (R package version 2.62.0, Bioconductor, 2025). https://github.com/federicomarini/topGO.
100. S. Sayols, rrvgo, A Bioconductor package for interpreting lists of Gene Ontology terms. *MicroPubl. Biol.* 10.17912/micropub.biology.000811 (2023).
101. B.T. Larson, Regulated development of cannibalistic supergiant cells. figshare. https://figshare.com/projects/Regulated_development_of_cannibalistic_supergiant_cells/261083. Deposited 19 August 2025.